Modeling and Analysis of Silicon Reflective-type Microring Resonator Assisted MZI as Filtering Device

Esraa M. El-edresee[1], Alhuda A. Al-mfrji[2]

Authors affiliations:

1) Department of Laser and Optoelectronics Engineering, College of Engineering, Al-Nahrain University, Baghdad, Iraq.
esraa.m.saeed@ced.nahrainuniv.edu.iq.

2) Department of Laser and Optoelectronics Engineering, Al-Nahrain University, Baghdad, Iraq.
alhuda.a.oied@nahrainuniv.edu.iq.

Abstract

Recently microwave photonic filter (MPF) have a great interest due to their advantages which include low loss, wide bandwidth tunability, reconfigurability, and no electromagnetic interference. This paper presented a comprehensive optical transmission analysis of a reflective-type microring resonator (R-MRR) using coupled mode theory, and design guidelines for MPF through two cascaded R-MRR using COMSOL software simulation results. The design was implemented on silicon-on-insulator (SOI) platform-based MPF which exhibits wide bandwidth tunability and reconfigurability by adjusting the coupling coefficient in the two coupling regions. In this structure, a grating coupler (GC) reflector is introduced to the drop port of MRR. The analysis and simulation results were confirmed by utilizing a GC reflector and Mach-Zehender Interferometer (MZI). The results of the proposed MPF at laser light input of (1.55*10^6- m) wavelength showed the bandwidth and center frequency are adjusted from 0.3 to 6 GHz and 13 to 54.8 GHz, respectively, with a high rejection ratio reaching 70 dB. Overall, the structure represents a significant step towards designing the MPFs, which show perfect flexibility and have numerous applications in such fields as radar, sensor, and wireless communications.

Keywords: Microwave Photonic Filter, Reflective-Type Microring Resonator, Silicon-On-Insulator, Mach-Zehender Interferometer.

نمذجة وتحليل مرنان السيليكون الميكروي من النوع العاكس بمساعدة MZI كجهاز ترشيح

اسراء محمد سعيد الادريسي، الهدى عبد الحسين المفرجي

الخلاصة:

في الآونة الأخيرة، حظي المرشح الضوئي بالموجات الدقيقة (MPF) باهتمام كبير نظرًا لمزاياه التي تشمل الفقد المنخفض وقابلية ضبط عرض النطاق الترددي الواسع وقابلية إعادة التشكيل وعدم وجود تداخل كهرومغناطيسي. قدمت هذه الورقة تحليلاً شاملاً للإرسال البصري لمرنان الرنين الميكروي من النوع العاكس (R-MRR) باستخدام نظرية الوضع المزدوج، وإرشادات التصميم لـ MPF من خلال اثنين من R-MRR المتتاليين باستخدام نتائج محاكاة برنامج COMSOL. تم تنفيذ التصميم على MPF القائم على منصة السيليكون على العازل (SOI) والذي يعرض إمكانية ضبط عرض النطاق الترددي الواسع وقابلية إعادة التشكيل عن طريق ضبط معامل الاقتران في منطقتي الاقتران. في هذا الهيكل، يتم إدخال عاكس المقرنة الشبكية (GC) إلى منفذ إسقاط MRR. تم تأكيد نتائج التحليل والمحاكاة باستخدام عاكس GC ومقياس تداخل Mach-Zehender Interferometer (MZI). أظهرت نتائج MPF المقترح عند ادخال ضوء الليزر بطول موجي يبلغ (1.55 * m 6^10) يظهر تعديل عرض النطاق الترددي والتردد المركزي من ٠,٣ إلى ٦ جيجا هرتز ومن ١٣ إلى ٥٤,٨ جيجا هرتز على التوالي، مع نسبة رفض عالية تصل إلى ٧٠ ديسيبل. بشكل عام، يمثل الهيكل خطوة مهمة نحو تصميم MPFs، والتي تظهر مرونة مثالية ولديها العديد من التطبيقات في مجالات مثل الرادار وأجهزة الاستشعار والاتصالات اللاسلكية.

1. Introduction

Microwave Photonic (MWP) on a Chip has been made possible by the exponential growth of incorporated semiconductor technologies [1]. Therefore, it was noticeable in recent years there has been a great development in microwave filtering applications due to its advantages in reducing power,

size, and cost [2,3]. The MPF excelled with broad bandwidth tunability, reconfigurability, and immunity to electromagnetic interference (EMI) [4-7]. Currently, MPFs are designed on several platforms such as SOI, silicon nitride, As2 S3, indium phosphide, and lithium niobate [8-10]. The most promising photonic integration platforms in the last decade are those based on silicon photonics. This is mostly due to the availability of complementary metal-oxide-semiconductor (CMOS) fabrication technology in conjunction with an extremely high index contrast [11-13]. Integrated microwave photonic filters (IMWP) are photonic subsystems that are intended to perform functions analogous to those of a conventional microwave filter while also bringing additional benefits specific to photonics. One of the most important and desired characteristics of IMWP is a high bandwidth selectivity, or the capacity to firmly reject adjacent channels which represents tunability and reconfigurability [14]. Therefore, MPF is used in important communications applications such as sensors, radar, and wireless communications [15,16].

Several technological options have been described to achieve excellent tunability and reconfigurability, including phase-shifted Bragg gratings [17], ring-assisted MZI topologies [18], and high-order micro-ring resonator MRR-based designs [19]. By including MRRs in the configuration of the MZI, it is possible to develop filters that carry out the appropriate signal shaping. Each arm of the MZI has a nonlinear phase response, which enables the elimination of tiny frequency bands from a wide range [20]. Moreover, because of their small footprints and simple structural design, MRRs and MZIs are frequently chosen for the realization of tunable photonic filters by adjusting the coupling coefficients. The reflective-type MRR reduces the chip footprint and the total number of heater controls by using the same MRR for a two-stage filter, which makes it possible for a more reliable on-chip system than conventional MRRs [21-24].

This work focuses on a thorough examination of MPFs with small size, low power, wideband tunability, reconfigurability, and high rejection ratio using mathematical analysis and modeling. Two cascaded R-MRRs assisted MZI couplers that integrate the single-mode and multi-mode waveguide designs are used to create the MPF. On the SOI platform, the suggested gadget is used with a high index contrast. The reflective-type MRR reduces the chip footprint, reuses the same MRR for a two-stage filter, and allows for flexible adjustment of the bandwidth by controlling the coupling coefficients. The corresponding results are based on the simulation which is run by COMSOL software version 6.1. The goal of this work is to present a built model platform for filtering as well as analyzing the intensity transmission of R-MRRs to characterize the performance of the suggested device. After comparing simulation results for two, and three cascaded MRRs, the best results are shown when using two rings, in which the bandwidth are modified the FWHM and the center of frequency from 0.3 to 6 GHz and 13 to 54.8 GHz, respectively with low power and small size. During the tuning range, the maximum rejection ratio reached 70 dB.

2. Proposed Reflective-type MRR as MPF
2.1 Operation Principle

Microwave photonics, as the name implies, is a mix of disciplines where the interaction of microwave and optical signals are investigated for many applications, including radar, sensors [15], broadband access networks, filters, antennae arrays, fiber-to-the-home, satellite communication, etc. In this device, SOI platform is suggested with silicon (n=3.47) represents the core surrounded by silicon oxide represents cladding (n=1.45) which shows high index contrast and compactness. This design combines multi-mode waveguides that are represented in the ring and single-mode waveguides that form the MZI which is the result of reducing the higher-order mode and scattering losses.

In this work, the optical transmission of laser light input at the wavelength (1.55μm) investigated after passing through the add-drop MRR assisted two MZI. The operation principle of the proposed device is shown in Fig. 1. In the CW laser light, microwave signals are modulated by an electro-optic (E/O) modulator. After the optical wave passes through the optical bandpass filter (OBPF) which represents the proposed device, the signal is modified to the desired spectral content and then turned by the converter to the electrical signal which is called the optical to-electrical (O/E) converter. Thus, the transmission spectrum of the OBPF is measured, and so achieved the MPF by MRR with an MZI coupler with an anti-reflection grating coupler (GC).
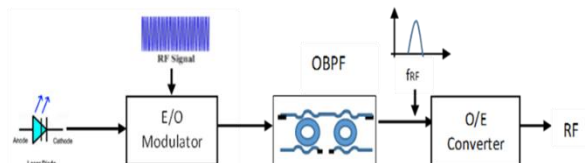

Figure (1): The implementation concept of the suggested MPF based on reflector R-MRRs optical waveguide.

Through the use of MRR in conjunction with a two-balanced MZI coupler and GC reflector, the MPFs are intended to provide bandwidth tunability and reconfigurability. The property of the proposed filter is to select the desired spectral content and control the bandwidth tunability and reconfigurability. This tuning process is achieved by simply applying a suitable voltage in the microheaters in the arms of MZI coupler [5].

2.2 Device Design and Analysis

The specifications and measurement of the proposed MPF based on the strong confinement SOI platform are produced. Furthermore, the theoretical framework and performance analysis required to design the reflective type MRR are given. The filter is implemented by using cascaded reflective-type MRR integrated with an MZI coupler. Through utilizing the reflective-type MRR, tunable bandwidth of MPF with a small footprint and more stable chip are established. The findings can be applied as a model to create small,

low-loss MPF with a wide tuning range and excellent reconfigurability.

2.2.1 Architecture

Reducing waveguide loss caused by scattering, coupling, and sidewall roughness is important in designing MRR. Therefore, the proposed device is structured as the model shown in Fig. 2a. In our design, two MZI are made with thin core waveguide width (0.5 μm) consisting of three angles 60° with a bending radius (20 μm) that formed two single-mode waveguides. In addition, multi-mode is represented in wide core waveguide widths (2 μm) with a bending radius (120 μm) and an angle of 120° as shown in Fig. 2b. In this geometry, linear adiabatic taper sets between MZI coupler and MRR waveguides with (40 μm) length. This means for both single-mode and multi-mode waveguides, the input and output core widths must be proportionate to their core widths [5]. In addition, four straight waveguides represent the input and output ports of MRR. The ring radius is equal (R=124 μm) from the ring's center to the wide waveguide's core. The separation between coupling regions (Gab) is equal (0.3 μm). Microheaters are set on two arms of MZI and in MRR to adjust the coupling coefficient and resonant wavelength.

In this device, a reflector is proposed as a grating coupler with a taper length of (5μm) and the opening angle of the taper is (17°) making light reflection back at the waveguide into a positive scattering angle as shown in Fig. 2c [25]. The most important thing that affects the coupling mechanism is applying electric potential in the microheaters deposited in the two arms of MZI that make a phase difference, which improves bandwidth reconfigurability on the MPF.

2.2.2. Characteristics of the Device Waveguide

In this model, we use an Electromagnetic Wave Beam Envelopes (ewbe) interface that is combined with Electrostatics to perform simulations of an optical waveguide filter at 1.55 wavelength by using the COMSOL software. Electrostatics are added to apply an electric field across the two arms of the MZI to make a phase difference that changed the coupling coefficients. The ewbe is the product of a slowly varying field (Amplitude) and a rapidly varying phase Ø which is defined the electric field. The ring curvature radius R and the separation distance between the straight and ring waveguide (dy) are very important parameters to define the wave propagation through the waveguide. x and y are the direction of the propagation waves in the x and y coordinate. The definitions for the phase used in the straight and ring waveguide are shown in these three equations:

- The phase definition in the two straight waveguides = Ø *x.
- The phase definition in the upper ring waveguide = Ø * R * atan2 ((y-R-dy), x).
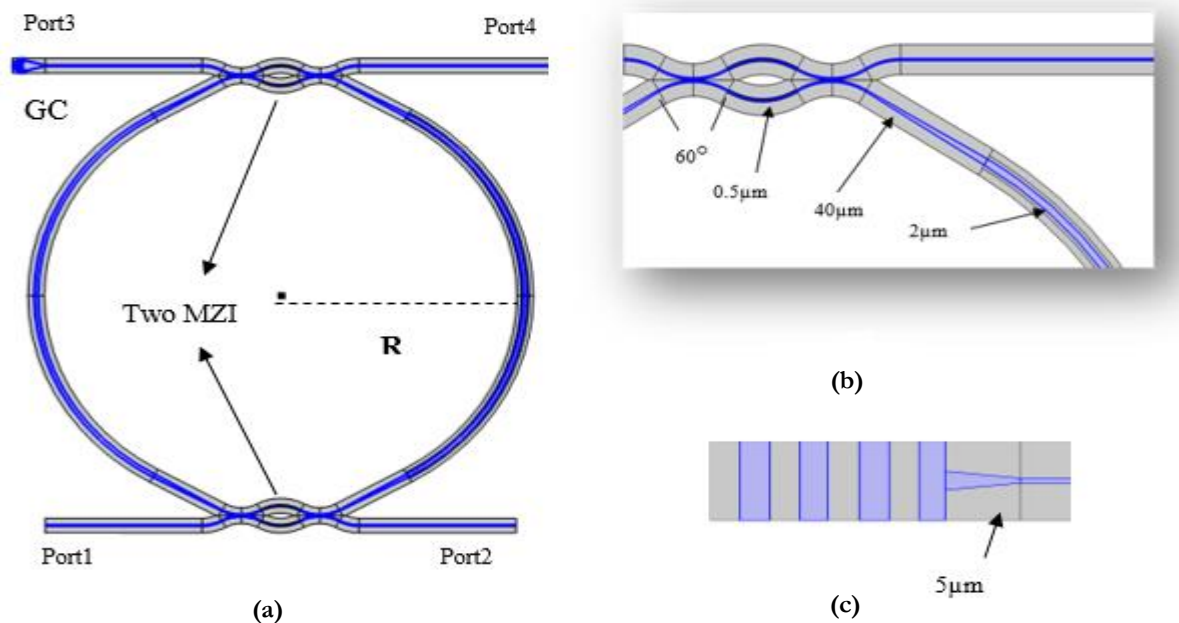- The phase definition in the lower ring waveguide = Ø * R * atan2 (-(y-R-dy), x).

Figure (2): Schematic diagram of proposed R-MRR: **(a)** Schematic diagram of proposed R-MRR with two MZI and GC; **(b)** Zoom in the tapper that connecting between wide and thin waveguide; **(c)** Schematic diagram of grating coupler.

Thus, it represents the discontinuous connection between the straight and ring waveguides. To sit continual phase and field, field continuity boundary conditions are used between two of these waveguide cores to ensure continuous electric and magnetic fields, while the phase is jumped. In Fig. 3, clarified microheaters that set the coupling coefficients through controlling the applied voltage. Therefore, the refractive index changes due to the applied electric field and thus results in changing the phase of a wave passing through the waveguide.

In the proposed device, a symmetrical MZI coupler implemented to adjust the coupling coefficients between the two coupling regions which makes phase variations in the lower and upper arms by setting electric potential and ground which

represent microheaters on the waveguides of the MZI. This gives rise to an equivalent coupling coefficient by adjusting the applied voltage on upper and lower arms of the MZI.
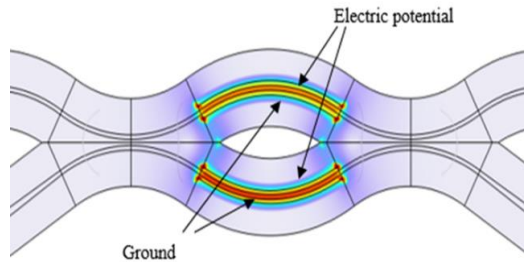

Figure (3): The structure of (MZI) coupler with set of microheaters in the two arms.

When the core waveguides are placed close together, the light waves are coupled and interfere constructively. In this design, three important things must be adjusted in the general parameters to satisfy the equivalent coupling between the two coupling regions:

- The first parameter was the radius of the microring must be set exactly from the ring center to the core waveguide which is represented as (R= 80*wavelength) that equals 124 µm.
- Secondly, the coupling gap that represent (dy=distance between the straight waveguide and the ring) which is equal to 0.3 µm according to (dy = 0.6*core width).
- The important thing that affects the coupling mechanism is applying electric potential that makes a phase difference and adjusting the coupling coefficients between the two arms of MZI, which improves bandwidth tunability and reconfigurability on the MPF.

To accurately simulate the suggested device, the edge mesh as shown in Fig. 4 are specified. The mesh size is divided by wavelength to get the maximum mesh element sizes. It is important to use the finite element method in the frequency domain when designing the R-MRR as a bandpass filter, thus the frequency with the S-parameter on the dB scale are simulated to very fine steps in the ports, S11 is the import, and S21, S31, S41 is the output port. As a result, a smooth curve like a Gaussian pulse is obtained as a function of frequency when the effective refractive index is sweep.
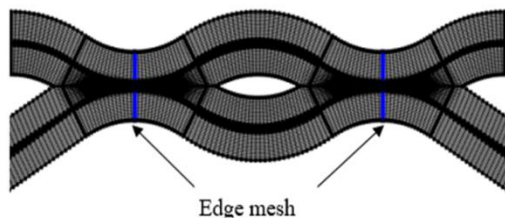

Figure (4): Zoom-in edge mesh of MZI by COMSOL software.

2.2.3 Analysis of an Add-Drop Reflector MRR with MZI coupler

In this design, MRR with a grating coupler reflector are proposed. Besides, to adjust the coupling coefficients, two symmetric MZI with four microheaters are employed as shown in Fig. 5 to modulate the bandwidth reconfigurability of the proposed MPF.

A single microring resonator, two straight optical waveguides, and a GC reflector attached to the drop port make up an add-drop MRR with a reflector. Light is coupled into the ring waveguide and transmitted through port 3 in a counterclockwise (CCW) direction when an optical signal is injected into the MRR through input port 1 [21–22]. When the circumference of the ring L equals an integer multiple of the entire wavelength, the coupling resonance condition is satisfied. The coupling resonance condition is written as:

$$Ln_{eff} = m\lambda_m \qquad \dots (1)$$

Where:

$$L = 2\pi R \qquad \dots (2)$$

Thus, R is the radius of the MRR; n_{eff} is the effective refractive index of the waveguide; m is an integer mode number; λ_m is the resonance wavelength. Where E_1 is the continuous input optical amplitude of port 1, E_2 and E_4 are the output signal of the optical amplitude at port 2 and port 4, respectively. E_3 is the reflected input wave by the GC reflector that has reflectivity η which is presented in port 3. The complex amplitude is referred to in E_{1a}, E_{2a}, E_{3a}, and E_{4a} as shown in Fig. 5a. In this design, the attenuation coefficient inside the ring waveguide is expressed with the symbol α. The phase variation in the four arms of the two MZI couplers is expressed with ΔØ as shown in Fig. 5b. Where Ø is the optical phase shift determined by the propagation constant β and L as:

$$\emptyset = \beta L \qquad \dots (3)$$

To resolve the interchange of optical power between optical waveguide MZI and ring waveguide, the coupling region proposed to be lossless coupler, and this is represented in t² + k² =1. For suitability of the design and computation, the self-coupling coefficient t and cross-coupling coefficient k of the MZI coupler are designed identically shown in Fig. 6, respectively. Where t* and k*are the complex conjugate of two coupling coefficients which are equal t*= -t and k*= -k.
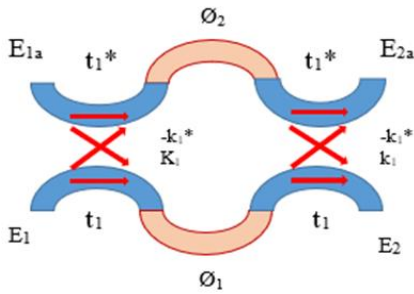

(a)
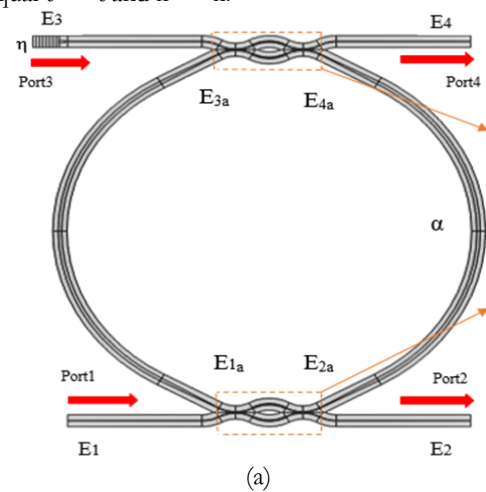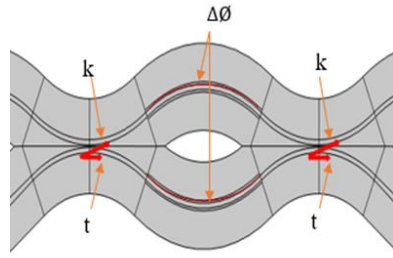
(b)

Figure (5): The schematic analysis of the proposed device; **(a)** The electric field of the MRR with two MZI couplers; **(b)** Zoom-in view of the balanced MZI coupler.
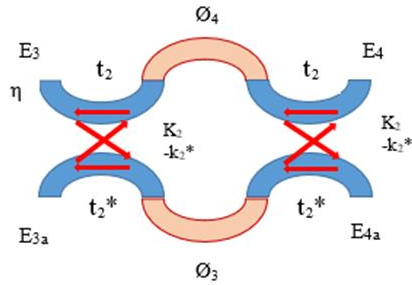
(a)

(b)

Figure (6): The schematic diagram of the two-coupling region based on a balanced MZI coupler; **(a)** lower MZI coupler; **(b)** upper MZI coupler.

From all mentioned above and based on Fig. 6a and 6b, we can describe the transfer matrix of two MZI coupling regions in the following [26]:

$$\begin{pmatrix} E_2 \\ E_{2a} \end{pmatrix} = \begin{pmatrix} t_1 e^{-i\emptyset_1} & k_1 \\ -k_1* & t_1*e^{-i\emptyset_2} \end{pmatrix}\begin{pmatrix} t_1 & k_1 \\ -k_1* & \alpha t_1* \end{pmatrix}\begin{pmatrix} E_1 \\ E_{1a} \end{pmatrix} \quad \dots (4)$$

$$\begin{pmatrix} E_{4a} \\ E_4 \end{pmatrix} = \begin{pmatrix} \alpha t_2* & -k_2* \\ \alpha k_2 & \eta t_2 e^{-i\emptyset_4} \end{pmatrix}\begin{pmatrix} \alpha t_2*e^{-i\emptyset_3} & -k_2* \\ \alpha k_2 & t_2 \end{pmatrix}\begin{pmatrix} E_{3a} \\ E_3 \end{pmatrix} \dots (5)$$

R-MRR is utilized in this structure in conjunction with a symmetrical MZI coupler. This arrangement enables high-Q resonators that can change the phase difference between the upper and lower arms of the MZI by adjusting the coupling coefficient in the coupling area with regard to the applied voltage in the microheaters. Thus, the tunability and reconfigurability of the integrated bandpass filter MPF can modify precisely. Where $\Delta\emptyset$ is the phase modulation of the 2×2 MZI coupler [27]. The electric

field E1 is slowly varying amplitude A at the time **t** of the frequency ω of the optical signal which is expressed in:

$$E_1 = Ae^{\wedge}i\omega\boldsymbol{t} \quad \dots (6)$$

and A is defined as:

$$A = (1 - t_1 t_2 \alpha e^{-i\emptyset}) \quad \dots (7)$$

The intensity response is characterized by analyzing the electric field in the proposed device according to the dynamic of microring resonator theory [28] shown in Fig. 6a and 6b from the import to the outport:

$$E_2 = (t_1 e^{-i\Delta\emptyset_1} \times E_1 + k_1 e^{-i\Delta\emptyset_2} \times E_{1a}) \dots (8)$$

$$E_{2a} = ((-k_1*)e^{-i\Delta\emptyset_1} \times E_1 + (t_1*)e^{-i\Delta\emptyset_2} \times E_{1a}) \dots (9)$$

$$E_3 = (\alpha k_2 t_2 e^{-i\Delta\emptyset_3} \times E_{4a}) \quad \dots (10)$$

$$E_{3a} = (\alpha(t_2*)(-k_2*)e^{-i\Delta\emptyset_3} \times E_{4a}) \quad \dots (11)$$

From the GC reflector, we can obtain the reflectivity in the port 4:

$$E_4 = (\eta t_2 e^{-i\Delta\emptyset_4} \times E_3 + \alpha k_2 \times E_{4a}) \quad \dots (12)$$

$$E_{4a} = (\alpha e^{-i\theta} \times E_{2a}(\boldsymbol{t} - \tau)) \quad \dots (13)$$

Where E_{4a}, τ, and θ represent the electric field inside the ring, propagation time coupler, and propagation phase shift, respectively. If there are no losses in the coupling regions, we obtain $t_2^2 + k_2^2 = 1$ and $t_1^2 + t_2^2 = 1$.

The intensity transmission T when the light travels from port 1 to port 3 can be expressed in the square of the electric field ratio between E_1 and E_3:

$$T_{31} = \left|\frac{E_3}{E_1}\right|^2 = \frac{(\sqrt{\alpha}t_2 k_2 e^{-i\Delta\emptyset_3} \times E_{4a})^2}{(1-\alpha t_1 t_2 e^{i\emptyset})^2} = \frac{\alpha(1-t_1^2)(1-t_2^2)(E_{4a})^2}{1-2\alpha t_1 t_2 cos\emptyset + (\alpha t_1 t_2)^2} \quad \dots (14)$$

The equation for the intensity transmission from port 3 to port 4 can be expressed as follows:

$$T_{43} = \left|\frac{E_4}{E_3}\right|^2 = \frac{(\eta t_2 e^{-i\Delta\emptyset_4} \times E_3 + \sqrt{\alpha}k_2 \times E_{4a})^2}{\alpha(1-t_1^2)(1-t_2^2)(E_{4a})^2} \quad \dots (15)$$

Then, we can simplify Eq. (15) to:

$$T_{43} = \left[\frac{(\eta t_2 e^{-i\Delta\emptyset_4})^2(E_3)^2}{\alpha(1-t_1^2)(1-t_2^2)(E_{4a})^2} + \frac{(\sqrt{\alpha}k_2)^2(E_{4a})^2}{\alpha(1-t_1^2)(1-t_2^2)(E_{4a})^2}\right] \quad \dots (16)$$

$$T_{43} = \left|\frac{E_4}{E_3}\right|^2 = \left[\eta^2 t_2^2 + \frac{k_2^2}{(1-t_1^2)(1-t_2^2)}\right] \quad \dots (17)$$

From Eq. (14) and (17), the intensity response of the proposed R-MRR from port 1 to port 4, expressed in:

$$T_{41} = \left|\frac{E_4}{E_1}\right|^2 = \frac{\eta^2(1-t_1^2)+(1-t_2^2)}{1-2\alpha t_1 t_2 cos\emptyset + (\alpha t_1 t_2)^2} \quad \dots (18)$$

By utilizing the R-MRR, reconfigurable and tunable MPF can be established with a small footprint and more stable chip. The optical signal in the GC port is reflected back and constructively interferes with the looping amplitude in the ring which results in tunning the coupling coefficient.

Furthermore, the coupling length needs to be appropriately built in accordance with the MRR's resonant wavelength. To enable complete reflection of the light wave, the design sets the coupling length of the optical coupler to fulfil a 50:50 coupling rate [21]. Asymmetric MZIs with two microheaters deposited on two arms are also used to modify the coupling coefficients. To investigate that, Eq. (4) is simplified which represents the transfer matrix of the lower MZI region. Therefore, by taking the square of the output electric field in Eq. (9), we can get:

$$T = \sqrt{(k_1^2\,(E_1)^2 + t_1^2(\,E_{1a})^2)} + \sqrt{(2k_1t_1E_1E_{1a}COS(\Delta\emptyset_1 - \Delta\emptyset_2)} \quad \dots (19)$$

According to Eq. (19), by varying the phase difference through the two arms of MZI, the coupling coefficients are adjusted inside the ring. By controlling the electrical power applied to the microheaters the phase difference can changed. Therefore, the transmission response is tuned.

3. Simulation Results

Precise consideration is given to designing MPF with bandwidth monitoring based on sequential R-MRR and MZI. The proposed MPF is supported by MZI coupler and GC reflector which is demonstrated on strong confinement SOI platform [29]. The simulation results are reported by COMSOL version 6.1 software to get a clear comparison picture between two, and three R-MRRs and finally choose the desired results represented in two cascaded R-MRRs with low power and loss, smaller size, and wide bandwidth tunability and reconfigurability. The structure size is 0.3×0.6 mm as shown in Fig. 7.
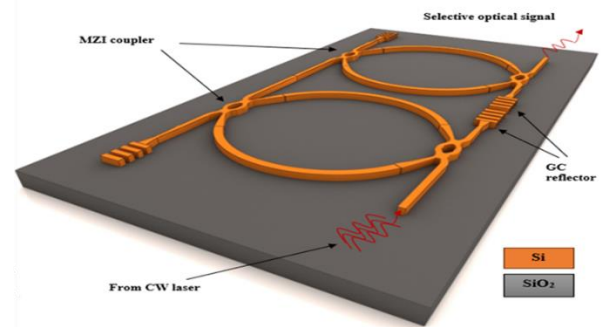

Figure (7): 3D Structure of the proposed two cascaded R-MRR.

A three-dimensional structure is performed as shown in Fig. 8a using the COMSOL software and illustrates a zoom-in view of the grating coupler reflector. The most important parameters that affect the coupling mechanism which is implemented in this design are the reflectivity from the grating coupler reflector and the phase shift in the upper and lower arms of MZI as shown in Fig. 8c which shows the length of the gap between the two coupling regions that bring out the wide bandwidth tunability and reconfigurability. Fig. 8b shows a linear diabatic taper waveguide that is connected between the single-mode waveguide (SMW) and multimode waveguide (MMW) which reduces the loss and avoids generating high mode.
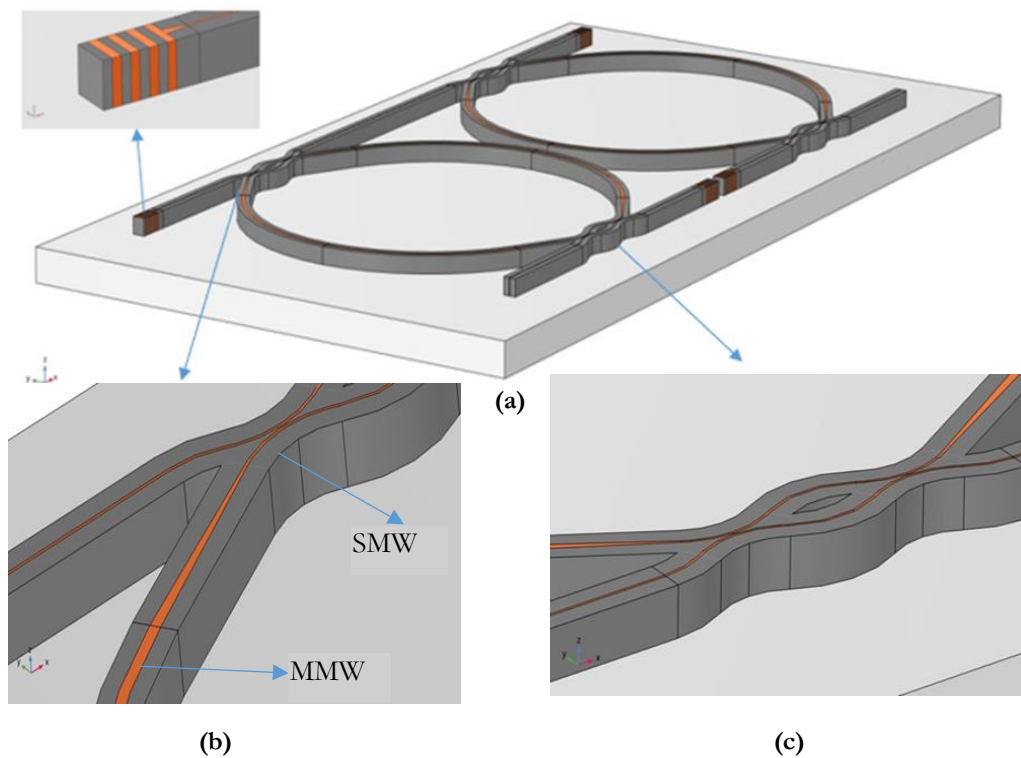

Figure (8): 3D structure of MPF for two cascaded R-MRR using COMSOL: **(a)** 3D of the proposed device and a zoom-in view of the grating coupler reflector; **(b)** A zoom-in linear diabatic taper waveguide which connected between (SMW) and (MMW); **(c)** The two coupling regions of MZI.

A CW laser light at 1550 nm wavelength is introduced into the proposed structure during the silicon waveguide and the output is selective of the desired spectral content. The MRR assisted MZI coupler waveguide is described by an effective refractive index and phase shift which is voltage dependent, which is applied to the microheaters in the lower and upper arm of the MZI. Further, the phase modulated changed the coupling coefficients which modified the transmission response, therefore adjusted the bandwidth tunability and reconfigurability of MPF. The parameters that are used in the design are listed in the Table (1).

Table (1): Parameters values used in COMSOL program.

Parameters	Value
MZI silicon waveguide width (µm)	0.5
MRR silicon waveguide width (µm)	2
silicon waveguide height (µm)	0.22
SiO_2 waveguide height (µm)	2
SiO_2 length (µm)	300
SiO_2 width (µm)	600
Taper of MRR length (µm)	40
Taper of GC length (µm)	5
Bending radius of wide width waveguide (µm)	120
Bending radius of thin width waveguide (µm)	20

After the optical wave injected to port 1, the optical signal transmitted and coupled to the ring through the resonance condition as shown in Fig. 9, which is satisfied when the circumference of the ring equals an integer multiple numbers of the whole wavelength.
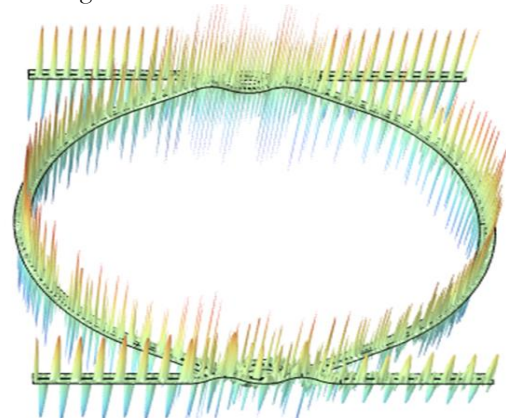

Figure (9): The electric field inside the MRR after satisfied resonance condition.

3.1 Simulation Results for two R-MRRs

The two R-MMR shown in Fig. 10 consists of two MRRs with four GC reflector, four MZI coupler, and eight microheaters (Mh) that placed on each arm of MZI coupler with input power port 1W.
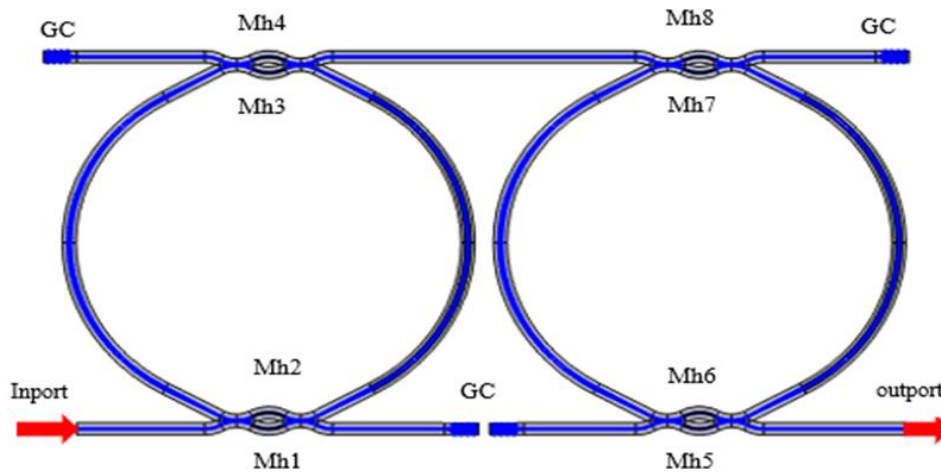

Figure (10): Schematic diagram of two R-MRR with GC reflector.

Taking into consideration the voltage applied to the microheaters was inserted to adjust the bandwidth reconfigurability and tunability. The GC in the proposed device is designed with a forward scattering, that makes optical signal scattered into a positive scattering angle. The bandwidth reconfigurability obtained by increasing the applied voltage on microheaters deposited on the upper and lower arms of the MZI. After setting the applied voltage to 1.5 v, the transmission spectrum was measured from the outport. The results showed that bandwidth reconfigurability with a flat top was achieved at 4 GHz after increasing the voltage applied on the microheaters to 4.5 v. Meanwhile, from a group of refractive indices the best confinement is satisfied in refractive indices (2.5, 2.502, 2.508). Therefore, the highest optical transmission with 0 dB insertion loss satisfied in (2.509) refractive index.

Adjusting the resonant wavelength and coupling coefficients by changing the applied voltage of the two R-MRR, brings about reconfiguring the bandwidth from 0.3 to 6 GHz with RR more than 60 dB as shown in Fig. 11(a). By using optical to electrical technique, the center frequency can be tuned from 13 to 54.8 GHz by adjusting the resonant wavelengths as shown in Fig. 11(b).

The relationship between the applied voltage of the microheaters and the FWHM of the two consecutive R-MRR is illustrated in Fig. 12a. To improve the Q factor of the optical filter for two cascaded R-MRRs, the MPF was set at the narrowest bandwidth of 0.3 GHz. The Q-factor and waveguide loss are 1.9×10^2 and 0.17 dB, respectively.

Meanwhile increasing the bandwidth to 1.0 GHz, the rejection ratio is decreased to 68.5 dB. Furthermore, the insertion loss is increased to 2.5 dB and the measured SNR is 47.5 dB. Fig. 12b shows the

rejection ratio and the SNR of the MPF at 1 GHz for two cascaded R-MRR. The decrease in the rejection ratio is proportional to the tuning of the MRRs, which also increases the insertion loss of the structure. The measured finesse is 33.3×10^2 for the two cascaded R-MRRs.

By using optical to electrical techniques, the center frequency can be setting from 13.2 to 54.8 GHz. The tuning range is restricted by the bandwidth of the phase modulator. Monitoring the wavelength and coupling coefficients of the two cascaded reflective type MRRs brings the bandwidth of the optical bandpass MPF reconfigured from 0.3 to 6 GHz with a high rejection ratio. Taking into consideration that the FSR of the proposed instrument is 100 GHz (0.8 nm), the Finesse parameter can be identified as the ratio of the FSR to the FWHM for characterizing a resonator's performance.
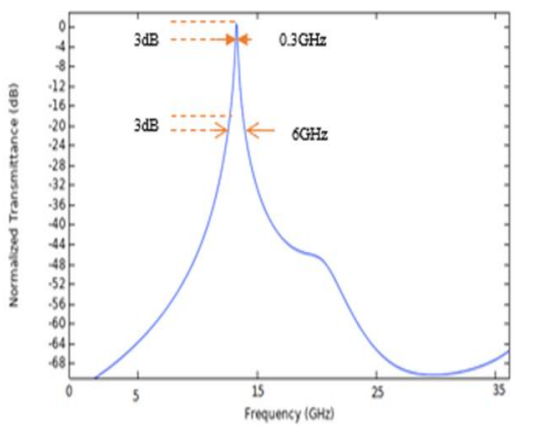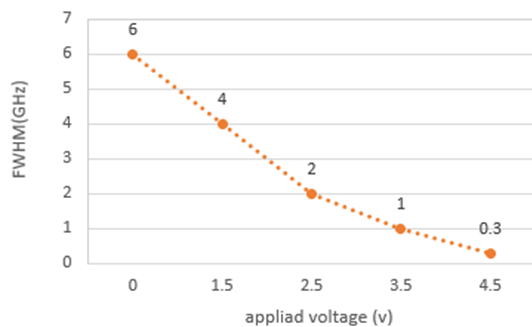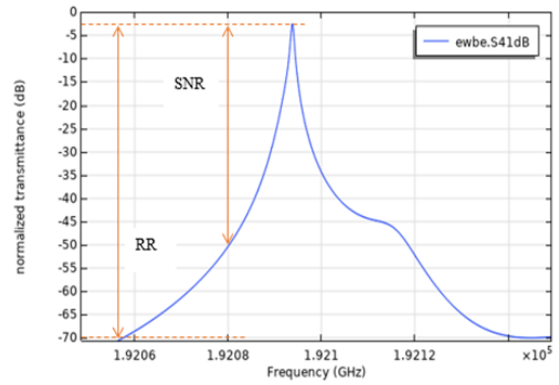

(a)
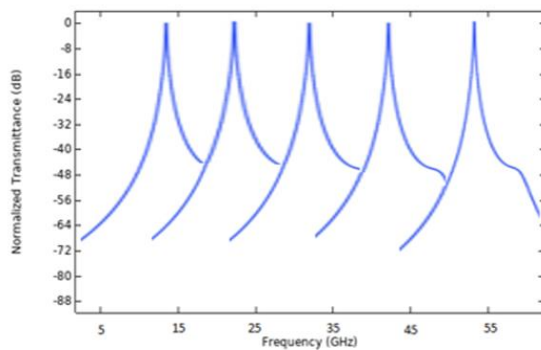
(b)

Figure (11): Measured and simulated frequency response of MPF for two R-MRR as: **(a)** Adjusting the bandwidth from 0.3 to 6 GHz; **(b)** Tuning the center frequency from 13.39 to 54.8 GHz.

(a)

(b)

Figure (12): Measured and simulated transmission of MPF for two R-MRRs **(a)** The bandwidth variation in two cascaded R-MRRs concerning changing the applied voltage in the microheaters **(b)** Measured rejection ratio and signal to noise ratio of MPF at 1 GHz.

3.2 Simulation Results for three R-MRRs

The design of MPF with three MRRs has six GC and MZI coupler. The MRR1 connected with MRR2 and MRR3 through a straight waveguide length of 190 μm to avoid side coupling. The higher optical transmission investigated with less insertion loss from a group of refractive indices which represent the best confinement that makes the light flow inside the wave guide in very small radii.

The input power is 1W taking into consideration the applied voltage in the 12 microheaters deposited in the lower and upper arms of the MZI to adjust the bandwidth reconfigurability. Between a group of refractive indices from 2.35 to 2.65, the highest frequency response with an insertion loss of 9.2 dB was achieved in 2.541. The measured optical transmission spectrum for three R-MRRs from outport is shown in Fig. 13. By controlling the applied voltage, the coupling coefficients were adjusted resulting in the bandwidth being reconfigured from 0.2 to 6 GHz and the tuning range from 45 to 66 GHz with more than 60 dB rejection ratio.
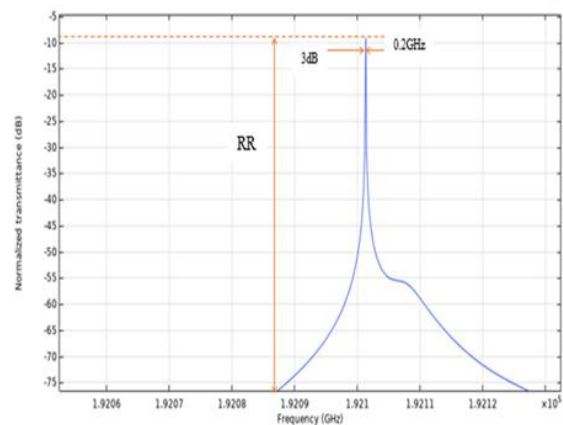

Figure (13): Measured transmission spectrum of three R-MRRs with 0.2 FWHM.

Fig. 14. showed the structure design of 3 MRR. Cascading more microrings, increasing the waveguide loss due to scattering and sidewall roughness loss.
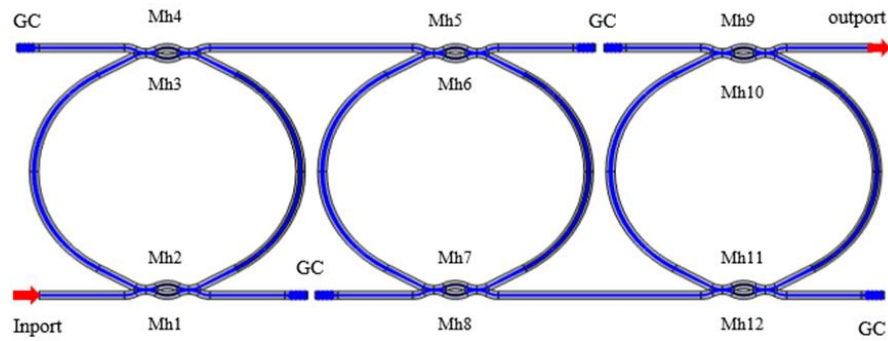
Figure (14): Schematic diagram of three R-MRRs with GC reflectors.

Furthermore, there is a drawback represented in the high voltage applied to the microheaters due to the number of microheaters that are used in this design. The Q factor and Finesse are characterized in this design, increasing the number of rings raising the quality factor, and finesse to reach are 2.25×10^2 and 5×10^2 respectively.

In order to obtain an MPF with a small size, less loss, low voltage, wide tuning range, and to keep pace with the development taking place in optical electronic devices, two and three cascaded R-MRRs rings were designed to obtain the best results. After comparison in these terms, the design with two rings obtained the best results in size, loss, and approximately a higher adjustment of the bandwidth tunability and reconfigurability. In addition, the comparison between formerly recorded integrated microwave photonic bandpass filters with the proposed device is represented in Table (2). This new MPF showed excellent reconfigurability with highest rejection ratio during previously integrated bandpass MPFs with different techniques. Overall, this design represents significant step towards designing the MPFs, which show perfect flexibility and has numerous applications in such fields as radar, sensor, and wireless communications.

Table (2): Performance Comparison of MPFs With Different Technology.

Technology	Platform	Filter Type	Reconfigure (GHz)	Rejection Ratio (dB)	Tuning Range (GHz)
DR-MZIs [31]	Si_3N_4	Bandpass	0.79-8.87	20	2-9
MMR [32]	SOI	Bandpass	0.17	26.5	2-18.4
MRR & MZI [30]	Si_3N_4	Bandpass	2-7	20	5-6
MRR [11]	SOI	Bandpass Bandstop	0.97-0.84	62	5-35
R-type MRR & MZI [24]	SOI	Bandpass Bandstop	3-78	60>	37.7-95.2
MRR & MZI [5]	SOI	Bandpass	0.7-2	51	5.2-35.8
R-type MRR & MZI (This work)	SOI	Bandpass	0.3-6	70	13-54.8

4. Conclusions:

This work presents a detailed design methodology for an optical bandpass filter based on a two-cascaded reflective-type microring resonator waveguide incorporation SOI platform. Performance predictions have been presented for the silicon reflector ring designed for 1550 nm wavelength. The key role played by combining features of two methods, using the MZI coupler with MRR and adding the GC reflector to the drop port of add-drop MRR has been identified in detail.

The design and performance of a reflective-type microring resonator as a filtering device was described. The structure characteristics are clarified and the simulation results are brought to light. The design integrated a single-mode waveguide formed MZI coupler and multi-mode waveguide with GC connected to the MRR. The features of the new MPF represented low insertion loss, small size, low power, and wide tuning range

5. Suggestions for Future Work:

This work can be extended in the future to cover the following issues:

1-To extend the design methodology of the proposed MPF with another platform such as Lithium niobate which took a great stride toward compact photonic integrated circuits.

2-To use MRR with a different ring size within reason the resonance amplitude was suitable to the size of the ring resonator.

3-To design a silicon MRR-assisted MZI with different coupling gaps between the coupling region to achieve the optimum coupling condition by modifying the phase difference.

4-To use more than three cascaded R-MRRs such as five cascaded rings and compare the filtering device performance with results reported.

5-Use another reflector technique such as a looped mirror, or metal film, or change the measurement in the grating coupler and compare the reflectivity parameters with the results in the proposed device.

6. References:

[1] J. Capmany, B.Ortega, D. Pastor, A tutorial on microwave photonic filters, J. Light. Technol 24 (2006) 201-229.

[2] Y. Tao, H.Shu, X.Wang, M.Jin, Z.Tao, F.Yang, J.Shi, J.Qin, Hybrid-integrated high-performance microwave photonic filter with switchable response, Photonics Res 9 (2021) 1569.

[3] H.Yang, J.Li, G.Hu, B.Yun, Y.Cui, Hundred megahertz microwave photonic filter based on a high Q silicon nitride multimode microring resonator, OSA Contin 3 (2020) 1445.

[4] F.M.Geremew, S.Talabattula, Performance analysis of reconfigurable multifunctional photonic filters using triple coupled microring resonators, Opt. Commun. 486 (2021) 126800.

[5] Y.Liu, Y.Chen, L.Wang, Y.Yu, Y.Yu, X.Zhang, Tunable and Reconfigurable Microwave Photonic Bandpass Filter Based on Cascaded Silicon Microring Resonators, J. Light. Technol. 40 (2022) 4655–4662.

[6] L.Wang, Y.Liu, Y.You, W.He, Xi.Xu, L.Feng, W.Geng, X.Chou, Microwave photonic filter with a sub-kHz bandwidth based on a double ring Brillouin fiber laser, Opt. Lett. 47 (2022) 4143.

[7] Z.Tao, Y.Tao, M.Jin, J.Qin, R.Chen, B.Shen, Y.Wu, H.Shu, S.Yu, X.Wang, Highly reconfigurable silicon integrated microwave photonic filter towards next-generation wireless communication, Photonics Res.11 (2023) 682–694.

[8] S.Song, S.X.Chew, X.Yi, L.Nguyen, R.A.Minasian, Tunable single-passband microwave photonic filter based on integrated optical double notch filter, J. Light. Technol.36 (2018) 4557–4564.

[9] D.Marpaung, C.Roeloffzen, R.Heideman, A.Leinse, S.Sales, J.Capmany, Integrated microwave photonics. Nature Photon. 13 (2012) 80-90.

[10] Y.Liu, A.Choudhary, G.Ren, K.Vu, B.Morrison, A.Casas-Bedoya, T.G.Nguyen, D.Y.Choi, P.Ma, A.Mitchell, S.J.Madden, D.Marpaung, B.J.Eggleton, Integration of Brillouin and passive circuits for enhanced radio-frequency photonic filtering, APL Photonics 4 (2019) 106103.

[11] W.Jiang, L. Xu, Y.Liu, Y.Chen, X.Liu, J.Yi, Y.Yu, Y.Yu, X.Zhang, Optical filter switchable between bandstop and bandpass responses in SOI wafer, IEEE Photonics Technol. Lett. 32 (2020) 1105–1108.

[12] W.Shan, L.Lu, X.Wang, G.Zhou, Y.Liu, J.Chen, L.Zhou, Broadband continuously tunable microwave photonic delay line based on cascaded silicon microrings, Opt. Express 29 (2021) 3375.

[13] W.Bogaerts, P.D.Heyn, T.V.Vaerenbergh, K.D.Vos, S.Kumar, Silicon microring resonators. Laser Photonics Rev. 6 (2021) 47–73.

[14] R.Sabella, Silicon Photonics for 5G and Future Networks, IEEE J. Sel. Top. Quantum Electron.26 (2020) 8301611.

[15] L.Xu, Xiao.H, Y. Zhang, J.Yi, Y.Yu, X. Xiao ,Y.Yu, A highly sensitive and precise temperature sensor based on optoelectronic oscillator, Opt. Commun. 483 (2021) 4655.

[16] L.Liu, X.Jin, T.Ning, L.R.Chen, J.Capmany, Optical Spectral Slicing Based Reconfigurable and Tunable Microwave Photonic Filter, J. Light. Technol. 38 (2020) 5492–5499.

[17] C.Fang, V.R.Shrestha, I.A.Ukaegbu, G.Ren, S.Pan, B.Nakarmi. Ultra-compact wideband filter with sidelobe suppression based on double modulated grating-assisted microring resonator, Opt. Contin.1 (2022) 623.

[18] Y.Chen, L.Xu, W.Jiang, L.Wang, S.Cui, Y.Yu, Y.Yu, X.Zhang, Reconfigurable second-order optical all-pass filter, Nanophotonics 11 (2022) 3115–3125.

[19] L.Xu, J.Hou, H.Tang, Y.Yu, Y.Yu, X.Shu, X.Zhang, Silicon-on-insulator-based microwave photonic filter with widely adjustable bandwidth, Photonics Res.7 (2019) 110.

[20] Y.Xie, Y.Shi, L.Liu, J.Wang, R.Priti, G.Zhang, O.Liboiron-Ladouceur, D.Dai, Thermally-Reconfigurable Silicon Photonic Devices and Circuits. IEEE J. Sel. Top. Quantum Electron. 26 (2020).

[21] S.Pan, Z.Tang, M.Huang, S.Li, Reflective-Type Microring Resonator for On-Chip Reconfigurable Microwave Photonic Systems, IEEE J. Sel. Top. Quantum Electron, 26 (2020).

[22] M.Huang, S.Li, Z,Yang, S.Pan, Analysis of a flat-top optical ring resonator, Opt. Commun. 451 (2019) 290–295.

[23] M.Huang, S.Li, M.Xue, L.Zhao, S.Pan. Flat-top optical resonance in a single-ring resonator based on manipulation of fast- and slow-light effects, Opt. Express 26 (2018) 23215.

[24] F.M.Geremew, T.Srinivas, Reflective coupled microring resonators for reconfigurable photonic systems: Performance analysis. Results Opt. 5 (2021) 100111.

[25] J.Hoffmann, K.M.Schulz, G.Pitruzzello, L.S.Fohrmann, A.Y.Petrov, M.Eich, Backscattering design for a focusing grating coupler with fully etched slots for transverse magnetic modes, Sci. Rep. 8 (2018) 1–8.

[26] X, Chen, L.Gu, P.Huang, X.Gan, N.Wang, Y.Zhu, J.Zhang, Optical transmission properties of si3 n4 add-drop micro-ring resonator induced by a fabry–perot resonance effect, Sensors 21 (2021).

[27] W.D.Sacher, J.K.S.Poon, Characteristics of microring resonators with waveguide-resonator coupling modulation, J. Light. Technol. 27 (2009) 3800–3811.

[28] W.D.Sacher, J.K.S.Poon, Dynamics of microring resonator modulators. Opt. Express 16 (2008) 15741.

[29] M.Pu, L.Liu, H. Ou, K.Yvind, J.M.Hvam, Ultra-low-loss inverted taper coupler for silicon-on-insulator ridge waveguide, Opt. Commun. 283 (2010) 3678–3682.

[30] Y.Zhao, X.Wang, D.Gao, J.Dong, X.Zhang, On-chip programmable pulse processor employing cascaded MZI-MRR structure, Front. Optoelectron. 12 (2019) 148–156.

[31] Q.Sun, L.Zhou, L.Lu, G.Zhou, J.Chen, Reconfigurable High-Resolution Microwave Photonic Filter Based on Dual-Ring-Assisted MZIs on the Si3N4 Platform, IEEE Photonics J. 10 (2018).

[32] H.Qiu, F.Zhou, J.Qie, Y.Yao, X.Hu, Y.Zhang, X.Xiao, Y.Yu, J.Dong, X.Zhang, A continuously tunable sub-gigahertz microwave photonic bandpass filter based on an ultra-high-Q silicon microring resonator, J. Light. Technol, 36 (2018) 4312–4318.